Non-Uniform Metamaterial Mushroom Antennas via a Genuine Multi-Objective Bayesian Optimization Method

Yunjia Zeng[1], Xianming Qing[1], Michael Yan-Wah Chia[1]
[1]Institute for Infocomm Research, A*STAR, Singapore; e-mail: {zeng_yunjia; qingxm; michael_chia}@i2r.a-star.edu.sg

***Abstract*— Three broadband non-uniform metamaterial mushroom antennas are designed with distinct mushroom configurations. The design trade-offs among the input impedance bandwidth, boresight gain, and the front-to-back ratio are considered with a genuine multi-objective Bayesian optimization method. The three non-uniform antennas attain a notable increase in impedance bandwidth with different degrees of trade-off in terms of the other two design targets when compared to the reference antenna with uniform mushroom configuration. All the four antennas are prototyped and measured, with strong alignment between simulation and measurement. The optimized designs can function in the n77 band of 5G New Radio.**

***Index Terms*—Mushroom Antenna, Microstrip Antenna, Multi-Objective Bayesian Optimization, Design Trade-off, 5G New Radio.**

I. Introduction

The 5G New Radio (NR) Frequency Range 1 (FR1) at sub-7 GHz includes n77 (3300–4200 MHz) is being widely adopted by different countries for the 5G networks [1]. Patch antennas have long been a popular choice for various communication systems due to the benefits of a compact profile and easy integration with systems. However, the applications of the classical microstrip antennas are constrained by their intrinsic narrow bandwidth. Periodic metamaterial mushroom antennas, as a type of microstrip antenna, can achieve improved bandwidth while still maintaining a relatively low profile. In [2], a 4 × 4 mushroom structure is fed with microstrip-line slot, and the TM_{10} and TM_{20} modes are simultaneously excited to attain broad bandwidth. With an antenna thickness of $0.03\lambda_0$, the periodic mushroom antenna achieves a fractional bandwidth of 14% with $|S_{11}| < -10$dB. In [3] and [4], by introducing shorting pins and etching slots, microstrip patch antennas with a profile of $0.032\lambda_0$ and $0.029\lambda_0$ achieve a fractional bandwidth of 15.2% and 13% respectively. Nevertheless, it is shown in study that to further increase the bandwidth, the height of substrate needs to be increased significantly [2]. Therefore, it is desirable to find solutions to further enhance the microstrip patch antenna's bandwidth without increasing the antenna profile.

An effective method for improving the bandwidth is to utilize non- uniform or non-periodic structures that can excite multiple resonances [5, 6]. The typical design method is to apply dispersion analysis to analyze a few element substructures, but it is difficult to explore the full potential of the non-uniform structures, which typically form a large design space because of the non-periodicity. Hence, it is advantageous to engage an optimization method for the design and tuning of the non-uniform metamaterial mushroom antennas. Bayesian optimization (BO) is well-suited for addressing challenges associated with intricate physical models and resource-intensive evaluation functions. It has found application in recent studies for the design and optimization of antennas [7, 8]. One crucial aspect of antenna design is the presence of multiple conflicting design targets, often requiring compromises as they cannot all be optimized simultaneously. In this context, a genuine multi-objective Bayesian optimization (MOBO) method [9] can be applied in antenna design for approximating the Pareto optimal set that captures different design trade-offs.

In this paper, a genuine MOBO method is employed for the design and optimization of non-uniform mushroom antennas for 5G New Radio. The MOBO approach is described with the design flow implemented. The captured design trade-offs are analyzed by comparing the three optimized non-uniform designs against their reference uniform counterpart with both the simulation and measurement results.

II. Design and Optimization

The reference antenna, a uniform 4 × 4 mushroom antenna, is designed based on [2], as shown in Fig. 1. The uppermost layer of the reference antenna comprises 16 mushroom cells, with each cell characterized by dimensions L_i and W_i. Every mushroom cell is linked to the middle layer's ground plane ($G_l \times G_w$) through vias with a diameter of d. The mushroom cells exhibit a periodicity denoted as p. The lower layer incorporates a microstrip feeding line with dimensions F_l for length and F_w for width. The antenna is fed by a slot ($S_l \times S_w$) located at the center of the ground plane. The PCB substrate applied is RO4003C. The detailed dimensions are listed in Table I. The reference antenna exhibits an input impedance bandwidth of 12.7% (3.46 GHz − 3.93 GHz), with a reflection coefficient lower than -10 dB. The study in [2] shows that by doubling the height, H_v, of the mushroom layer, the bandwidth can be increased from 14% to 22%. Such an

TABLE I. Dimensions of the Reference Antenna (in mm)

G_w	G_l	L_i	W_i	p	d
88	88	18	18	19	1
F_l	F_w	S_w	S_l	H_v	H_m
56	2	4	35	1.524	0.813

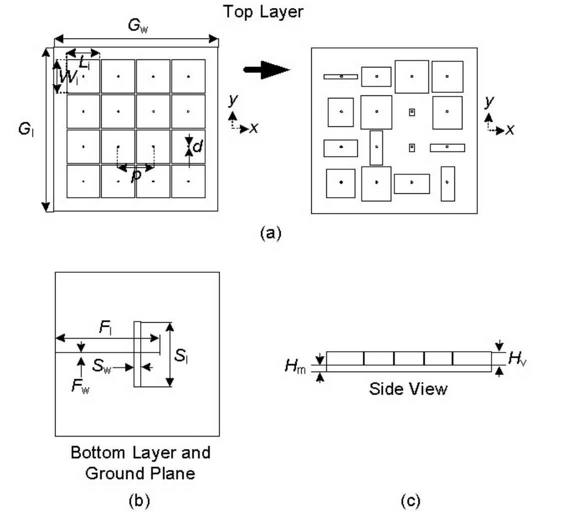

Fig. 1. Configurations of the uniform/non-uniform mushroom antenna: (a) top view; (b) bottom view; (c) side view.

approach, nonetheless, could compromise the low-profile advantage inherent to microstrip antennas. By incorporating non-periodicity into the mushroom structure, it becomes possible to induce multiple resonances, thus achieving a broader bandwidth. The non-uniform mushroom layer's design involves adjusting the length (L_i) and width (W_i) of all the sixteen mushroom patches. Together with the microstrip feeding line (F_l, F_w) and the feeding slot (S_w, S_l),

A. Two-Objective Design Problem

In the first non-uniform design, the width and length of all the 16 mushroom cells are to be tuned as shown in Fig. 1(a). The vector of 36 design variables is expressed as $\boldsymbol{x} = [L_1, W_1, L_2, W_2, \ldots, L_{16}, W_{16}, F_{L1}, F_{w1}, S_{L1}, S_{w1}]$.

In this scenario, the primary goal is to optimize the impedance bandwidth in the targeted frequency range of 3.3-4.2 GHz. Another performance metric taken into consideration is the realized gain at boresight in the frequency range. The optimization problem of this non-uniform mushroom antenna is formulated as follows:

$$\text{minimize } F_1(\boldsymbol{x}), F_2(\boldsymbol{x}) \quad \text{s.t. } \boldsymbol{x}^l \leq \boldsymbol{x} \leq \boldsymbol{x}^u, \qquad (1)$$

where

$$F_1(\boldsymbol{x}) = \frac{1}{m}\sum_{i=1}^{m} \max[S_{11}(\boldsymbol{x}, f_i) + 10, 0],$$

$$F_2(\boldsymbol{x}) = \frac{1}{n}\sum_{i=1}^{n} \max[10 - RG(\boldsymbol{x}, f_i), 0],$$

with $F_1(\boldsymbol{x})$ and $F_2(\boldsymbol{x})$ as the two real-valued objective functions, $\boldsymbol{x}^l$ and $\boldsymbol{x}^u$ formed by the lower and upper bounds of the design variables, m and n represent the number of points to sample in the targeted frequency band.

B. Three-Objective Design Problem

The second and the third non-uniform antenna designs are with different configurations of metamaterial mushroom structures. As shown in Fig. 2 (a), the second design has a mushroom layer that exhibits a concentric rectangular ring configuration. The inner four patches have the same size as (L_{in}, W_{in}), while the outer twelve patches are with the same dimensions of (L_{out}, W_{out}). Therefore, the second non-uniform design corresponds to a vector of 8 design variables as $\boldsymbol{x} = [L_{in}, W_{in}, L_{out}, W_{out}, F_{L2}, F_{w2}, S_{L2}, S_{w2}]$.

On the other hand, the third design has a rotational symmetric configuration, with the dimensions of each patch corresponding to ($L_{j,3}$, $W_{j,3}$), where j corresponds to the patch labels in Fig. 2(b). Thus, the input vector of this design contains 12 variables with $\boldsymbol{x} = [L_{1,3}, W_{1,3}, L_{2,3}, W_{2,3}, L_{3,3}, W_{3,3}, L_{4,3}, W_{4,3}, F_{L3}, F_{w3}, S_{L3}, S_{w3}]$.

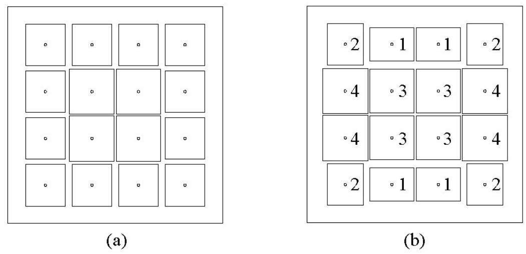

Fig. 2. Configurations of the top layers of: (a) the second and (b) the third non-uniform mushroom antennas.

For both the second and the third designs, the front-to-back ratio is also considered in the optimization, which can be formulated as

$$\text{minimize } F_1(\boldsymbol{x}), F_2(\boldsymbol{x}), F_3(\boldsymbol{x}) \quad \text{s.t. } \boldsymbol{x}^l \leq \boldsymbol{x} \leq \boldsymbol{x}^u, \qquad (1)$$

where

$$F_3(\boldsymbol{x}) = \frac{1}{p}\sum_{i=1}^{p} \max[10 - FtB(\boldsymbol{x}, f_i), 0],$$

with $F_1(\boldsymbol{x})$, $F_2(\boldsymbol{x})$ defined the same as in Section IIA, p being the number of sampling points of the front-to-back ratio in the frequency range.

C. Design and Optimization

In all the three non-uniform designs, the dimensions of each patch are varied in the range of [1, 18.5], to ensure there is no overlap between patches and to facilitate straightforward fabrication. The dimensions of the feeding line vary in the ranges of: $44 \leq F_{L1,2,3} \leq 74$, $1 \leq F_{w1,2,3} \leq 4$. The slot size of the first design is constrained as $20 \leq S_{L1} \leq 76$, $1 \leq S_{w1} \leq 17$. Since the slot size may have significant impact on the front-to-back ratio, the second and third designs with the front-to-back ratio taken into consideration have reduced dimension ranges as $20 \leq S_{L2,3} \leq 35$, $1 \leq S_{w2,3} \leq 4$.

A genuine MOBO method known as UseMO [9] is employed to address the design and optimization challenges of the non-uniform mushroom antennas. The design flow implemented is as depicted in Fig. 3. Firstly, the Latin Hypercube method is used to acquire samples across the design domain formed by the above-mentioned ranges. CST

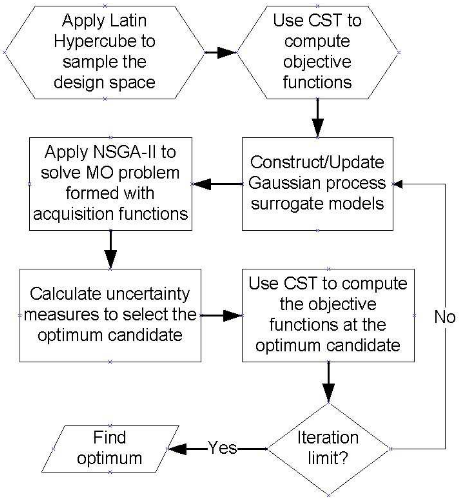

Fig. 3. Implemented design flow of UseMO.

simulations are then run on every sample to compute the performance metrics such as input reflection coefficients, realized gains, and front-to-back ratios, so that the objective functions corresponding to each sample can be calculated. The samples, along with their computed objective functions, are utilized to form a prior dataset for constructing probabilistic Gaussian process surrogate models for each corresponding objective function. At the outset of the iteration, acquisition functions are formulated for each of the surrogate models. NSGA-II is used to solve the multi-objective optimization problem formed with the acquisition functions as the objectives [10]. Subsequently, the uncertainty measures of the candidate points obtained from NSGA-II are determined [9], and the one with the highest uncertainty measure is selected as the best candidate and subsequently simulated in CST. The data generated from this new sample is then employed to update the Gaussian process surrogate models. Once the predetermined iteration limit is reached, all the simulated outcomes are gathered, leading to the attainment of optimized designs.

III. Results

For each of the three designs, a Pareto optimal set has been obtained. For non-uniform design I, the optimized design is chosen from the Pareto set such that it has the largest input impedance bandwidth and with a gain variation less than 3dB at boresight. The optimal non-uniform designs II and III are chosen such that they exhibit the largest impedance bandwidth with a front-to-back ratio greater than 10 dB within their respective Pareto sets. The dimensions of all the three optimized non-uniform designs are presented in Table II. All the four antenna prototypes are shown in Fig. 4. It is interesting to note that the non-uniform design II in Fig. 4(c) resembles the uniform design as the patch dimensions being similar.

As shown in Fig. 5(a), the designs achieve the measured bandwidth with $|S_{11}|$ < -10dB as follows: 3.46−3.96 GHz

TABLE II. Dimensions of the Optimized Non-uniform Antennas (in mm)

Non-uniform design I							
W_1	W_2	W_3	W_4	W_5	W_6	W_7	W_8
2.0	10.0	17.2	16.5	15.3	17.9	3.5	17.3
W_9	W_{10}	W_{11}	W_{12}	W_{13}	W_{14}	W_{15}	W_{16}
9.0	18.4	4.1	3.9	15.3	18.3	10.2	18.3
L_1	L_2	L_3	L_4	L_5	L_6	L_7	L_8
17.5	16.0	18.1	16.5	13.6	16.1	2.5	15.5
L_9	L_{10}	L_{11}	L_{12}	L_{13}	L_{14}	L_{15}	L_{16}
18.0	6.6	3.1	18.2	15.2	15.3	18.4	7.1
F_{L1}	F_{w1}	S_{L1}	S_{w1}				
54.7	1.0	41.7	16.7				
Non-uniform design II							
L_{in}	W_{in}	L_{out}	W_{out}	F_{L2}	F_{w2}	S_{L2}	S_{w2}
18.3	18.4	17.8	18.1	57.6	2.4	33.9	1.3
Non-uniform design III							
$L_{1,3}$	$W_{1,3}$	$L_{2,3}$	$W_{2,3}$	$L_{3,3}$	$W_{3,3}$	$L_{4,3}$	$W_{4,3}$
18.1	13.6	14.7	16.9	18.1	17.7	18.5	18.5
F_{L3}	F_{w3}	S_{L3}	S_{w3}				
55.7	3.2	34.9	1.5				

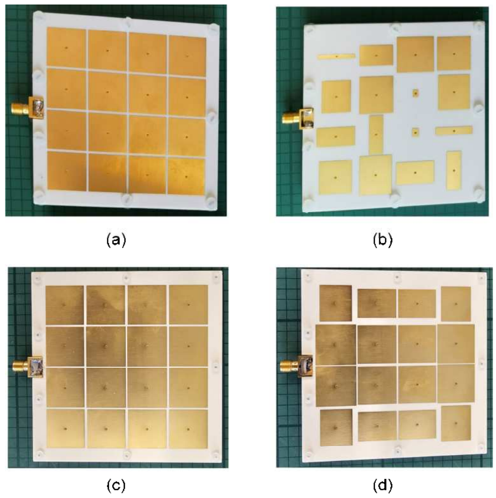

Fig. 4. Fabricated prototypes: (a) uniform reference; (b) non-uniform design I; (c) non-uniform design II; (d) non-uniform design III.

(13.5%) for uniform reference; 3.36−4.19 GHz (22.0%) for non-uniform design I; 3.45−4.08 GHz (16.7%) and 3.48−4.15 GHz (17.6%) for non-uniform designs II and III, respectively. It is important to highlight that the fractional bandwidth of all the three non-uniform designs achieves a significant increase as compared with that of the uniform reference. Figure 5(b) plots the simulated and measured boresight realized gain of all the designs, and it can be observed that the boresight realized gain of the non-uniform design I is much lower than that of the other three designs, while the uniform reference and the non-uniform designs II and III have peak realized gain close to each other. Over their impedance bandwidth, all the designs exhibit a stable realized gain with only a slight

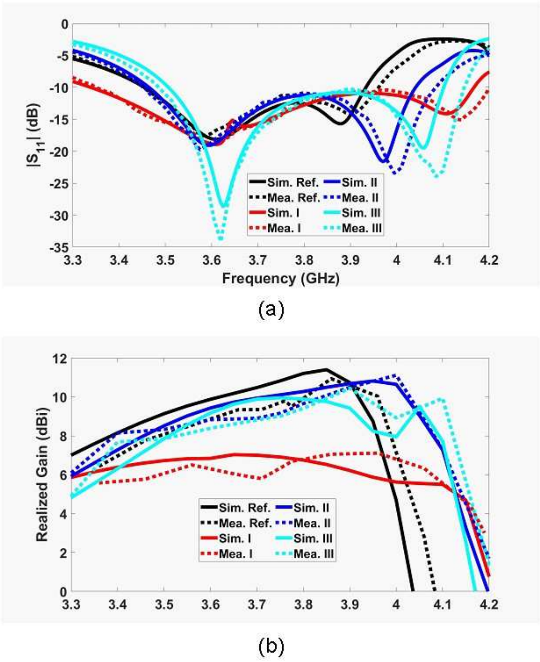

Fig. 5. Simulated and measured results of fabricated prototypes: (a) reflection coefficient; (b) realized gain.

drop near the higher band edge. The measurement and simulation results match well for all the antennas as shown in Fig. 5.

In Fig. 6, the radiation patterns of all the four designs are plotted at their corresponding center frequency. The measured radiation patterns are normalized and show good agreement when compared to the simulated patterns. Among the four designs, the uniform reference and the non-uniform designs II and III exhibit similar directional patterns, while the non-uniform design I has a broad beam and shows a strong backward radiation.

As for the non-uniform design I, only the return loss and realized gain were considered in the optimization, and there was no stringent constraint on the feeding slot size. Therefore, this design achieves the widest impedance where the large feeding slot plays a significant role in it. It also explains the relative low gain and strong backward radiation in this design.

During the optimization of the non-uniform designs II and III, the feeding slot size is restricted to being smaller than that of the uniform reference. Also, the front-to-back ratio is included as the third optimization target. From Fig. 6, it can be observed that the front-to-back ratio of these two non-uniform designs are comparable to that of the uniform reference. Therefore, these two non-uniform designs exhibit similar realized gain and front-to-back ratio but achieve a much wider bandwidth as compared with the uniform reference.

IV. Conclusion

A genuine multi-objective Bayesian optimization method has been employed to design and optimize three broadband

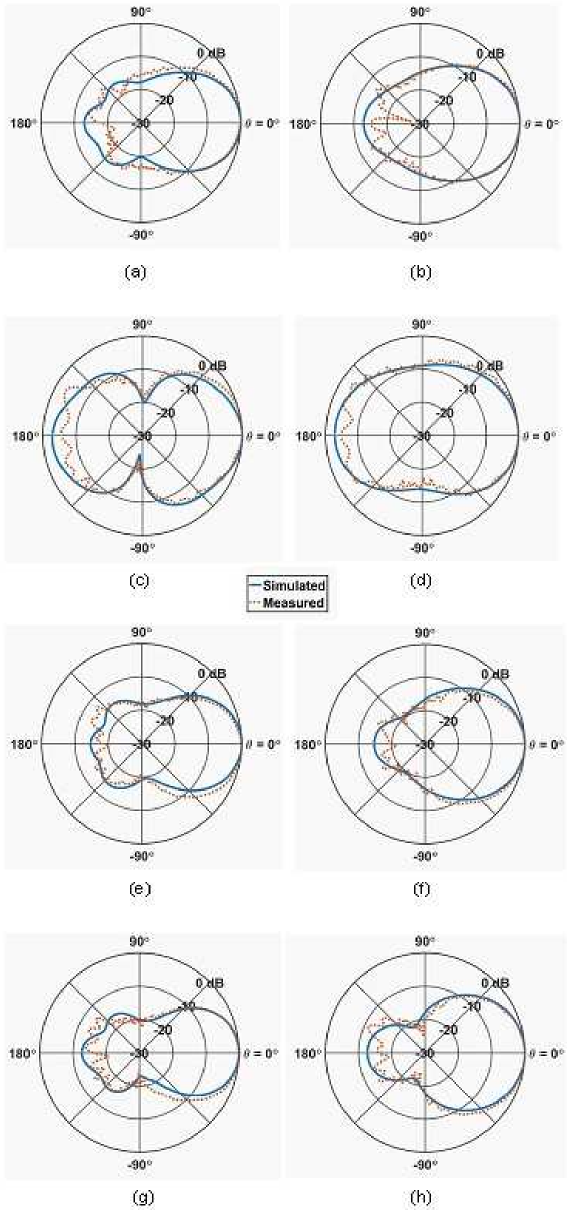

Fig. 6. Simulated and measured radiation patterns of the antennas at center frequency: (a) *xz*-plane of uniform reference; (b) *yz*-plane of uniform reference; (c) *xz*-plane of non-uniform design I; (d) *yz*-plane of non-uniform design I; (e) *xz*-plane of non-uniform design II; (f) *yz*-plane of non-uniform design II; (g) *xz*-plane of non-uniform design III; (h) *yz*-plane of non-uniform design III;

non-uniform mushroom antennas. All the three non-uniform antennas exhibit a noteworthy increase in input impedance bandwidth compared to the uniform reference, all retaining the low-profile characteristics as a microstrip antenna. Two-objective and three-objective optimization design flow have been implemented respectively. The inclusion of the additional objective, namely the front-to-back ratio, along with size constraints on the feeding slot, allow the non-uniform designs to preserve similar gain performance and directional patterns as the reference antenna. The genuine multi-objective

Bayesian optimization approach can be easily formulated to include additional design objectives, thereby enhancing the exploration of design trade-offs, and approximating the Pareto optimal set more effectively. The optimized antennas are validated at the popular FR1 n77 band in 5G New Radio.

ACKNOWLEDGMENT

This work was partially supported by the Agency for Science, Technology and Research (A*STAR), Singapore, under its AME YIRG Fund (A2084c0173).

REFERENCES

[1] "5G NR (New Radio)." [Online]. Available: https://www.etsi.org/deliver/etsi_ts/138100_138199/13810101/15.12.00_60/ts_13810101v151200p.pdf

[2] W. Liu, Z. N. Chen, and X. Qing, "Metamaterial-based low-profile broadband mushroom antenna," *IEEE Trans. Antennas Propag*., vol. 62, no. 3, pp. 1165–1172, Mar. 2014.

[3] N.-W. Liu, L. Zhu, W.-W. Choi, and J.-D. Zhang, "A low-profile aperture-coupled microstrip antenna with enhanced bandwidth under dual resonance," *IEEE Trans. Antennas Propag*., vol. 65, no. 3, pp. 1055–1062, Mar. 2017.

[4] N.-W. Liu, L. Zhu, and W.-W. Choi, "A differential-fed microstrip patch antenna with bandwidth enhancement under operation of TM10 and TM30 modes," *IEEE Trans. Antennas Propag*., vol. 65, no. 4, pp. 1607–1614, Apr. 2017.

[5] Y. Zeng, Z. N. Chen, X. Qing and J. Jin, "Design of a Near-Field Nonperiodic Zero Phase Shift-Line Loop Antenna With a Full Dispersion Characterization," *IEEE Trans. on Antennas and Propag*., vol. 65, no. 5, pp. 2666–2670, May 2017.

[6] W. Sun, Y. Li, Z. Zhang, and P.-Y. Chen, "Low-profile and wideband microstrip antenna using quasi-periodic aperture and slot-to-CPW transition," *IEEE Trans. Antennas Propag*., vol. 67, no. 1, pp. 632–637, Jan. 2019.

[7] A. Yang, W. Xue, C. Tian, J. Li, and L. Ye, "A Design of Silicon Based Horn Antenna Optimized Using Bayesian Optimization," in *Proc. Int. Conference on Computer and Communications (ICCC)*, Chengdu, China, 2020, pp. 438–442.

[8] J. Zhou et al., "A Trust-Region Parallel Bayesian Optimization Method for Simulation-Driven Antenna Design," *IEEE Trans. on Antennas and Propag*., vol. 69, no. 7, pp. 3966–3981, July 2021.

[9] S. Belakaria, A. Deshwal, N. K. Jayakodi, J. R. Doppa, "Uncertainty-aware search framework for multi-objective Bayesian optimization," in *Proc. of the AAAI Conference on Artificial Intelligence*, April 2020, Vol. 34, No. 06, pp. 10044–1005.

[10] K. Deb, A. Pratap, S. Agarwal and T. Meyarivan, "A fast and elitist multiobjective genetic algorithm: NSGA-II," *IEEE Transactions on Evolutionary Computation*, vol. 6, no. 2, pp. 182–197, April 2002.